Dalton Transactions

ROYAL SOCIETY OF CHEMISTRY

PAPER

View Article Online
View Journal | View Issue

Cite this: *Dalton Trans.*, 2024, **53**, 4772

Subtle adjustments for constructing multi-nuclear luminescent lanthanide organic polyhedra with triazole-based chelates†

Xiao-Qing Guo,[a] Li-Peng Zhou, [a] Shao-Jun Hu[a] and Qing-Fu Sun *[a,b]

Received 13th November 2023,
Accepted 29th January 2024

DOI: 10.1039/d3dt03791f

rsc.li/dalton

Controlled self-assembly of predetermined multi-nuclear lanthanide organic polyhedra (LOPs) still presents a challenge, primarily due to the unpredictable coordination numbers and labile coordination geometries of lanthanide ions. In this study, through introducing triazole-based chelates to increase the chelating angle of C_2-symmetric linear ligands and stabilize the coordination geometry of Eu(III) centers, M_4L_6-type (M = Eu^{III}, L = ligand) tetrahedra were efficiently synthesized, especially a biphenyl-bridged ligand which is well known to form M_2L_3-type helicates. A series of LOPs were formed and characterized by high-resolution electrospray ionization time-of-flight mass spectroscopy (ESI-TOF-MS) and X-ray crystallography. Moreover, the europium complexes exhibit bright emission (luminescence quantum yield up to 42.4%) and circularly polarized luminescence properties ($|g_{lum}|$ up to 4.5×10^{-2}). This study provides a feasible strategy for constructing multi-nuclear luminescent LOPs towards potential applications.

Introduction

Coordination-directed self-assembly is a compelling and versatile approach in the realm of supramolecular chemistry, holding significant promise for addressing the evolving needs of the scientific community.[1–5] Within this context, 3D metallosupramolecular architectures have emerged as intriguing candidates with diverse applications.[6–16] However, while the potential of coordination-directed self-assembly is evident, the utilization of lanthanide ions in constructing such assemblies, especially high-nuclear assemblies, has faced unique challenges.[17] Lanthanides exhibit remarkable spectroscopic and electromagnetic properties that make them attractive building blocks;[18–21] however, their application has been constrained by factors such as variable coordination numbers and low steric requirement. Inspired by the pioneering research conducted by Piguet,[22,23] Bünzli,[24] Gunnlaugsson,[25] Park[26] and others,[27–40] primarily including mononuclear bundles and dinuclear helicates, the field of lanthanide assembly chemistry has witnessed significant advancements. These achievements serve as valuable benchmarks, offering valuable insights and guidance for the future design and synthesis of more intricate and functionalized LOPs.[17,19,41–46]

Following the symmetry principles elucidated by Raymond's group,[47] our group published a structural evolution of $Ln_{2n}L_{3n}$ (Ln, lanthanides; L, ligands) edifices from helicates and tetrahedra to cubes by systematically increasing the offset between two chelating arms on C_2-symmetric bis(tridentate) ligands.[48] Notably, when compared to malposed C_2-symmetric ligands, linear ligands demonstrate greater ascendancy in maximizing the inner cavity volumes and window sizes of LOPs. However, the resulting structures assembled by linear amide–pyridine–amide ligands (APA-L, *e.g.*, chelating arms bridged by phenyl or biphenyl unit) and Ln^{III} are almost Ln_2L_3 helicates (Scheme 1).[49–52] In sharp contrast to Ln^{III} ions, the self-assembly of transition metal ions (M) with similar linear ligands typically results in the formation of M_4L_6 tetrahedra.[53] The underlying reason for this difference lies in the variable coordination configurations of Ln^{III} ions, a consequence of their unique electrostatic interactions, which result in a wide range of twist angles. Therefore, to construct Ln_4L_6 tetrahedra or higher-nuclear LOPs based on linear ligands, a rational strategy needs to be considered in the design of ligands.

According to Albrecht-Gary's report,[54,55] the self-assembly mechanism of triple-stranded helicates proceeds though a pre-organized "side-by-side" intermediate species, Ln_2L_2. Hence, the key to preventing the formation of low-nuclear Ln_2L_3 helicates lies in inhibiting the occurrence of the Ln_2L_2 intermediate, which can be achieved by enhancing the chelating angle and the ligand rigidity. To efficiently avoid the formation of

[a]*State Key Laboratory of Structural Chemistry, Fujian Institute of Research on the Structure of Matter, Chinese Academy of Sciences, Fuzhou 350002, P. R. China. E-mail: qfsun@fjirsm.ac.cn*
[b]*University of Chinese Academy of Sciences, Beijing 100049, PR China*

†Electronic supplementary information (ESI) available. CCDC 2304348–2304351. For ESI and crystallographic data in CIF or other electronic format see DOI: https://doi.org/10.1039/d3dt03791f

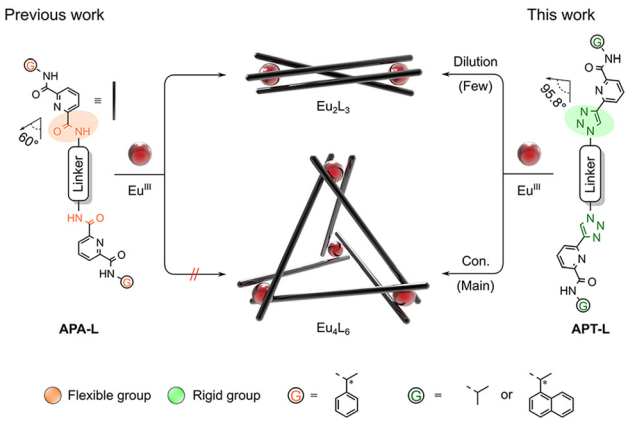

Scheme 1 Ligand modification for constructing multi-nuclear LOPs (Linker: phenyl/biphenyl/terphenyl; Con.: concentration).

Ln_2L_3, we have implemented two modifications to the ligands: (i) increasing the chelating angle and rigidity of C_2-symmetric linear ligands by introducing an amide–pyridine–triazole (APT) chelating arm and (ii) stabilizing the coordination geometry of the metal center by modifying the electron-rich naphthylethyl group on the periphery of the ligands (Scheme 1).

Herein, a series of LOPs were constructed by self-assembling APT-based C_2-symmetric ligands with Eu^{III} ions (Fig. 1). In contrast to our earlier findings and those of others,[48,50] we observed that linear ligands based on biphenyl spacers primarily formed Ln_4L_6 tetrahedra instead of the previously observed Ln_2L_3 helicates. This shift in preference can be attributed to the larger chelating angle, effectively inhibiting the formation of triple-stranded helicates. As a control experiment, isopropyl-modified $\mathbf{L_2}^{\mathbf{AC}}$ exhibited a tendency to form di-nuclear helicates relative to naphthylethyl-modified $\mathbf{L_2}^{\mathbf{RR/SS}}$, suggesting the feasibility of stabilizing the coordination geometry of the metal center through peripheral auxiliary groups. Furthermore, a significant $|g_{lum}|$ magnitude (4.5×10^{-2}) for $Eu_4(\mathbf{L_2}^{\mathbf{SS}})_6$ was observed in CPL spectroscopy, attributed to the enhanced metal coordination environment through inter-ligand synergistic effects.

Results and discussion

The APT-based bis(tridentate) ligands were synthesized in a three-step process: firstly, the chiral naphthylethyl group was attached to 6-bromopicolinic acid by amide coupling, followed by a Sonogashira-coupling reaction to introduce the alkyne group; then three spacers with different lengths bridged the chelating arms *via* a high-yield Cu(I)-catalyzed azide–alkyne cycloaddition (CuAAC) reaction.[56] All ligands were fully characterized using NMR and high-resolution ESI-TOF-MS spectra (see the Experimental section in the ESI† for details).

By simply increasing the linear length of the ligand, the assembly behavior of $\mathbf{L}_n^{\mathbf{RR/SS}}$ (n = 1–3) shows significant variations under the same conditions. When 3 eq. of $\mathbf{L}_n^{\mathbf{RR/SS}}$ (n = 1–3) were treated with 2 eq. of $Eu(OTf)_3$ in a CD_3CN/CD_3OD (v/v 4/1) mixture at 50 °C for several minutes, the initially turbid suspensions quickly turned into clear solutions. However, the architectural features of the resulting assemblies exhibited substantial diversity due to the inherent dissimilarities in the respective ligands.

In the case of $\mathbf{L_1}^{\mathbf{SS}}$ or $\mathbf{L_1}^{\mathbf{AC}}$, a singular set of ^{1}H NMR signals was observed, signifying the formation of a single species with high symmetry (Fig. 2A and B, S22 and S42†). Compared with free $\mathbf{L_1}^{\mathbf{SS}}$, most signals originating from the assembly experienced shifts attributed to the effects of lanthanide-induced shifts and relaxation rate enhancements.[57] The ^{1}H DOSY measurement of the solution showed that all signature signals had the same diffusion coefficient $D_1 = 5.68 \times 10^{-10}$ m^2 s^{-1},

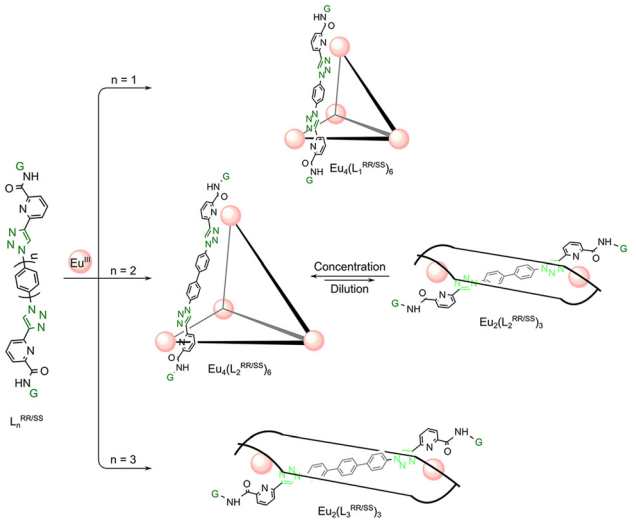

Fig. 1 The ligand length/concentration-dependent self-assembly behavior of linear C_2-symmetric bis(tridentate) ligands with $Eu(OTf)_3$.

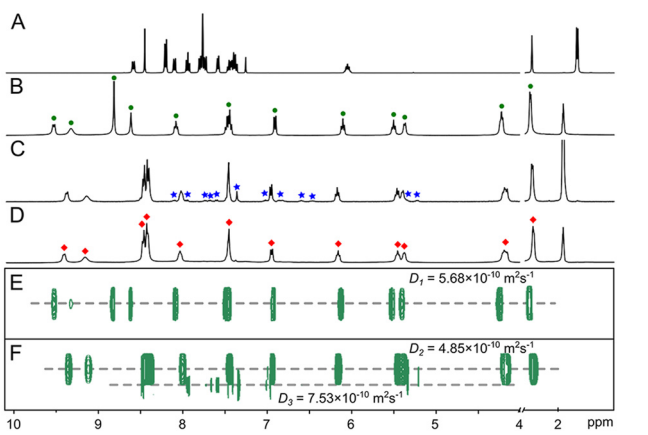

Fig. 2 ^{1}H NMR spectra (400 MHz, 298 K) of (A) $\mathbf{L_1}^{\mathbf{SS}}$ ($CDCl_3$), (B) $Eu_4(\mathbf{L_1}^{\mathbf{SS}})_6$ (●), the assemblies of $Eu(OTf)_3$ with $\mathbf{L_2}^{\mathbf{SS}}$ under different concentrations (C) 7.2×10^{-3} M, (D) 1.4×10^{-2} M (CD_3CN/CD_3OD, v/v 4/1, $Eu_2(\mathbf{L_2}^{\mathbf{SS}})_3$ (★), $Eu_4(\mathbf{L_2}^{\mathbf{SS}})_6$ (◆). ^{1}H DOSY of E) $Eu_4(\mathbf{L_1}^{\mathbf{SS}})_6$, and (F) the mixture of $Eu_2(\mathbf{L_2}^{\mathbf{SS}})_3$ and $Eu_4(\mathbf{L_2}^{\mathbf{SS}})_6$.

indicating the formation of a single species with a hydrodynamic diameter of 2.3 nm, estimated by the Stokes–Einstein equation (Fig. 2E). The composition of $Eu_4(\mathbf{L_1^{SS}})_6(OTf)_{12}$ in solution was further confirmed by ESI-TOF-MS analysis (Fig. S81†), which revealed a series of prominent peaks observed at m/z = 721.1652, 845.4669, 1011.2031, 1243.2347, and 1591.2808, corresponding well to $[Eu_4(\mathbf{L_1^{SS}})_6(OTf)_n]^{12-n+}$ (n = 4–8). It is worth noting that the assembly of APA-L, bridged by a biphenyl linker with a similar length of 16.5 Å (distance between pyridine nitrogen atoms, 16.0 Å for $\mathbf{L_1^{SS}}$ or $\mathbf{L_1^{AC}}$, Fig. S66†), only resulted in the triple helicate,[50] verifying the feasibility of chelating angle regulation for high-nuclear LOPs.

However, two sets of signals were observed during the assembly of $\mathbf{L_2^{SS}}$ (with an N⋯N distance of 19.5 Å) with Eu$(OTf)_3$, implying the possible presence of a mixture comprising $Eu_4(\mathbf{L_2^{SS}})_6$ and $Eu_2(\mathbf{L_2^{SS}})_3$ (Fig. 2C). This observation is consistent with the distinct diffusion coefficients observed in ^{1}H DOSY, where $D_2 = 4.85 \times 10^{-10}$ m^2 s^{-1} and $D_3 = 7.53 \times 10^{-10}$ m^2 s^{-1} (Fig. 2F). The composition of the mixture was also confirmed by ESI-TOF-MS (Fig. S82†). By integrating the ^{1}H NMR signals associated with $Eu_2(\mathbf{L_2^{SS}})_3$ and $Eu_4(\mathbf{L_2^{SS}})_6$ at a concentration of $[\mathbf{L_2^{SS}}]$ = 4.8 mM, the apparent equilibrium constant (K) for $2Eu_2(\mathbf{L_2^{SS}})_3 \rightleftharpoons Eu_4(\mathbf{L_2^{SS}})_6$ was determined to be 2.2×10^3 M^{-1} (ΔG = −19.1 kJ mol^{-1}, Fig. S55†). When the concentration of $[\mathbf{L_2^{SS}}]$ was increased from 4.8 to 14.4 mM, the complete transformation of $Eu_4(\mathbf{L_2^{SS}})_6$ was observed (Fig. 2D, S52†). In addition, once formed, the tetrahedral cage can maintain long-term stability under dilution conditions (3 days, conversion rate <25%, Fig. S53†). Furthermore, in comparison with $\mathbf{L_2^{AC}}$, it was observed that the assembly of $\mathbf{L_2^{SS}}$ tended to generate a higher proportion of tetrahedra under the same ligand concentration conditions (Fig. S54†). The corresponding apparent equilibrium constant (K) for $2Eu_2(\mathbf{L_2^{AC}})_3 \rightleftharpoons Eu_4(\mathbf{L_2^{AC}})_6$ was calculated as 39.4 M^{-1} (ΔG = −8.9 kJ mol^{-1}, Fig. S56†). Therefore, it can be inferred that the peripheral auxiliary group played a pivotal role in regulating the coordination geometry around the Eu^{III} center.

VT-NMR experiments were carried out to determine the thermodynamic parameters of the equilibria $2Eu_2(\mathbf{L_2^{AC}})_3 \rightleftharpoons Eu_4(\mathbf{L_2^{AC}})_6$ (1) and $2Eu_2(\mathbf{L_2^{SS}})_3 \rightleftharpoons Eu_4(\mathbf{L_2^{SS}})_6$ (2) using the van't Hoff equation (Figs. S57–S62†). The negative $\Delta G°$ values for the dimerization equilibria suggest that the transformation from helicates to tetrahedra is a spontaneous process at room temperature. To analyze the internal driving forces that regulate the helicate/tetrahedron equilibrium, the statistical factors ($\omega^{Eu,L_2^{AC}}{}_{dim}$ = 3/2 and $\omega^{Eu,L_2^{SS}}{}_{dim}$ = 3) and the corresponding free energy contributions ($\Delta G^{Eu,L_2^{AC}}{}_{dim}$ = −1.0 kJ mol^{-1} and $\Delta G^{Eu,L_2^{SS}}{}_{dim}$ = −2.7 kJ mol^{-1}) to equilibria (1) and (2) were calculated based on the literature[23] (see the detailed calculations in the ESI†). The negative free energies $\Delta G^{Eu,L}{}_{dim}$ indicate that the statistical factors favor the formation of tetrahedral cages due to the relaxation of the rotational degeneracy. Moreover, from a purely statistical point of view, $\Delta G^{Eu,L_2^{SS}}{}_{dim} < \Delta G^{Eu,L_2^{AC}}{}_{dim}$ demonstrates that the trend of dimerization in equilibrium (2) is stronger than that in equilibrium (1).

To quantitatively analyze the contribution of enthalpic/entropic driving forces to the dimerization process, the relationship between the dimerization constants ($\beta^{Eu,L}{}_{dim}$) and the effective molarities ($EM^{Eu,L}{}_{2,3}$) was deduced as $\beta^{Eu,L_2^{AC}}{}_{dim} = 3/2(0.71)^3/EM^{Eu,L_2^{AC}}{}_{2,3} = 0.54/EM^{Eu,L_2^{AC}}{}_{2,3}$ and $\beta^{Eu,L_2^{SS}}{}_{dim} = 3(0.75)^3/EM^{Eu,L_2^{SS}}{}_{2,3} = 1.27/EM^{Eu,L_2^{SS}}{}_{2,3}$, respectively.[23] Firstly, the term 3/2 or 3 from the statistical factors implies an entropic driving preference for the formation of tetrahedral cages, coinciding with positive $\Delta S°$ (0.016 kJ mol^{-1} K^{-1} and 0.030 kJ mol^{-1} K^{-1}) obtained by the VT-NMR experiments. Secondly, the transformation from triple-stranded helicates (30-membered metallomacrocycle, Fig. S65†) to tetrahedra (45-membered metallomacrocycle), accompanied by a reduction in enthalpic ring strain, further supports the favorability of the dimerization process. Experimental EM values at different temperatures were calculated to compare the relative trends for equilibria (1) and (2) (Table S1†). With the increase of temperature, the EM values showed a positive correlation, indicating that the temperature rise overcomes the gain of enthalpic ring strain and promotes the formation of helicates. Notably, the significantly lower $EM^{Eu,L_2^{SS}}{}_{2,3}$ compared to $EM^{Eu,L_2^{AC}}{}_{2,3}$ (about two orders of magnitude) indicates a stronger inclination of $[Eu_2(\mathbf{L_2^{SS}})_3]^{6+}$ to form tetrahedral cages. This preference may be attributed to serve ring strains or poor preorganization, which is consistent with the lower $\Delta H°$ = −9.923 kJ mol^{-1} of equilibrium (2) compared to $\Delta H°$ = −4.288 kJ mol^{-1} of equilibrium (1).

Given the high charge state of the complexes and the use of polar solvents, both the alterations in entropy and enthalpy largely depend on the change of solvent energies that can be evaluated by the Born equation.[58] The contributions of solvation energies ($\Delta_{solv}G^{Eu,L}{}_{4,6} - 2\Delta_{solv}G^{Eu,L}{}_{2,3}$) for equilibria (1) and (2) were determined to be −976 kJ mol^{-1} and −2777 kJ mol^{-1}, respectively. Therefore, considerable changes in solvation energies suggest a pivotal role in influencing the alterations of entropy and enthalpy during the dimerization process. Furthermore, from the perspective of solvation energies, the trend to form tetrahedra in equilibrium (2) emerges as notably more pronounced than that in equilibrium (1).

As anticipated, in the case of the extended-version ligand $\mathbf{L_3^{SS}}$ (with an N⋯N distance of 23.8 Å), it exclusively forms the $Eu_2(\mathbf{L_3^{SS}})_3$ helicate, which was confirmed by ^{1}H DOSY, NMR spectroscopy and ESI-TOF-MS (Figs. S38, S41 and S83†). These findings suggest that the strategy of regulating the chelating angle and coordination geometry configuration becomes unwieldy when using more flexible linear ligands.

Fortunately, colorless crystals suitable for X-ray diffraction analysis were obtained by the slow diffusion of dichloromethane vapour into the complex solution. In the case of $Eu_4(\mathbf{L_1^{RR}})_6$, a tetrahedral arrangement with approximate T symmetry was revealed, with four facially coordinated Eu^{3+} centers being bridged by six bis(tridentate) linear ligands (Fig. 3A). All Eu^{3+} centers adopt the same Λ configuration induced by the R, R-ligand point chirality. The average distance between two adjacent Eu^{III} centers was found to be 14.2 Å, defining a theoretically tetrahedral cavity of *ca.* 342 Å^3. Notably, intriguing

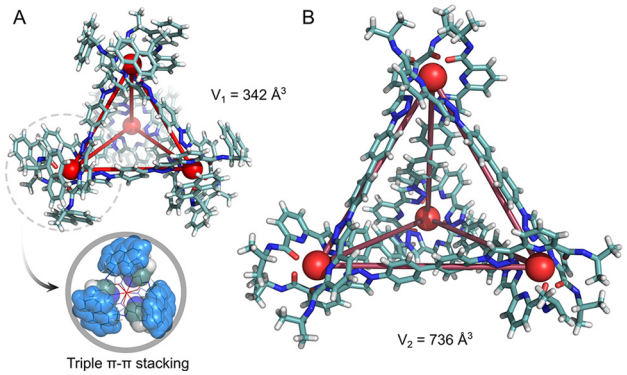

Fig. 3 Crystal structures of (A) $Eu_4(L_1^{RR})_6$ and (B) $Eu_4(L_2^{AC})_6$ (atom colours: red, Eu(III); blackish green, C; white, H; azarin, O; blue, N).

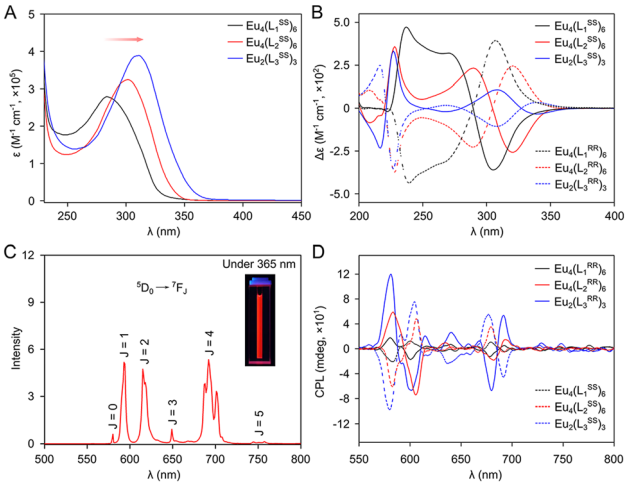

Fig. 4 (A) UV-Vis adsorption and (B) CD spectra of the assemblies in MeCN (1×10^{-5} M). (C) Emission spectrum of $Eu_4(L_2^{SS})_6$ excited at 331 nm with a photograph inset taken under 365 nm lamp. (D) CPL spectra of the assemblies in MeCN (1.0×10^{-5} M).

triple π–π stacking interactions were observed between the electron-rich naphthylethyl groups at the periphery and the electron-deficient pyridine groups from adjacent $\mathbf{L_1}^{RR}$ ligands. These interactions, resembling a mechanical contraction, appeared to enlarge the distance between the long arms of the complex, effectively preventing the formation of the helicate.

Regrettably, repeated attempts to crystallize $Eu_4(\mathbf{L_2}^{SS})_6$ were unsuccessful, possibly due to the low symmetry and the large cavity of the complex. As an alternative, a high-quality crystal structure for $Eu_4(\mathbf{L_2}^{AC})_6$ was obtained to unambiguously verify the tetrahedral architecture (Fig. 3B). In comparison with $Eu_4(\mathbf{L_1}^{SS})_6$, it is evident that the central cavity of the tetrahedron was significantly increased to 736 Å^3 (Fig. S71†) by extending the distance between the central Eu^{3+} ions to 18.5 Å. This expansion suggests its potential application in host–guest chemistry.

The UV-Vis absorption of $\mathbf{L}_n^{SS}$ (n = 1–3) and their corresponding assemblies was measured at room temperature (Fig. S72†). With the extension of the spacer, the aromaticity of the ligands was gradually increased, as evidenced by a noticeable bathochromic-shift in absorption (Fig. 4A). Circular dichroism (CD) spectroscopy was employed to verify the enantiomeric nature of the assemblies in solution. In the case of $Eu_4(\mathbf{L_2}^{SS/RR})_6$, the enantiomers exhibited a mirror image with a strong Cotton effect, manifesting as split peaks located at 221, 281 and 320 nm, corresponding to the UV-Vis region and arising from π → π* transitions (Fig. 4B). Similarly, the enantiomeric nature and optical activity of $Eu_4(\mathbf{L_1}^{SS/RR})_6$ or $Eu_2(\mathbf{L_3}^{SS/RR})_3$ were also confirmed by their CD spectra. The emission spectra of Eu^{III} assemblies were obtained in an acetonitrile solution. For $Eu_4(\mathbf{L_2}^{SS/RR})_6$, characteristic emission peaks were observed at 580, 594, 615, 649, 693 and 750 nm, corresponding to the $^5D_0 \rightarrow {}^7F_J$ (J = 0, 1, 2, 3, 4, 5) transitions (Fig. 4C). The excitation window for the $Eu_4(\mathbf{L_1}^{SS})_6$ cage is limited to <340 nm, while the $Eu_2(\mathbf{L_3}^{SS})_3$ helicate can be excited at 370 nm. Notably, except for $\mathbf{L_1}^{SS}$, highly efficient sensitization for Eu^{III} ions was demonstrated by the other two ligands. The quantum yields (Φ) of these supramolecular assemblies were determined to be 1.7% for $Eu_4(\mathbf{L_1}^{SS})_6$, 37.2% for $Eu_4(\mathbf{L_2}^{SS})_6$ and 42.4% for $Eu_2(\mathbf{L_3}^{SS})_3$ (Table S2†). Compared to analogous bis(tridentate) ligands featuring amide groups,[48,50,51] the rigid ligands with triazole-based chelates demonstrate enhanced efficacy in sensitizing the emission of europium ions. Typically, the quantum yields of the europium complexes with biphenyl-bridged bis(tridentate) ligands significantly increase from Φ < 1% to 37.2%. We speculate that the triazole group effectively suppresses the dissipation of energy transfer from the sensitizing group (biphenyl) to the Eu^{III} centers. Therefore, in addition to its effect on the assembly behavior, the triazole-based chelate group manifests a universally potent sensitizing performance for chiral europium complexes.

To analyze the origin of different quantum yields, the phosphorescence spectra of $Gd_4(\mathbf{L_1}^{SS})_6$, $Gd_4(\mathbf{L_2}^{SS})_6$, and $Gd_2(\mathbf{L_3}^{SS})_3$ were tested at 77 K under an N_2 atmosphere using a gating technique, from which the ligand triplet state energy levels $E_{0\text{–}0}(^3T)$ of $\mathbf{L}_n^{SS}$ (n = 1–3) were estimated to be 20 920, 20 790 and 19 342 cm^{-1}, respectively (Fig. S74†). The corresponding energy gaps of $E_{0\text{–}0}(^3T)$-$E(^5D_0)$ were determined to be 3720, 3520, and 2142 cm^{-1}, respectively. Generally, a larger energy gap implies a less favorable energy transfer from the ^3T to $^5D_0$ energy level. Consequently, the sensitization capability of ligands follows the sequence $\mathbf{L_3}^{SS}$ > $\mathbf{L_2}^{SS}$ > $\mathbf{L_1}^{SS}$. To further quantitatively compare the sensitization capabilities of ligands, the sensitization efficiency of ligands (η_{sens}) and the intrinsic quantum yield of europium (Q_{Ln}^{Ln}) are calculated (see the ESI† for details). The europium complexes demonstrate comparable intrinsic quantum yields: $Eu_4(\mathbf{L_1}^{SS})_6$, 42.4%; $Eu_4(\mathbf{L_2}^{SS})_6$, 43.3%; and $Eu_2(\mathbf{L_3}^{SS})_3$, 42.2%. Nonetheless, the η_{sens} of ligand $\mathbf{L_1}^{SS}$ (4%) is significantly lower than those of $\mathbf{L_2}^{SS}$ (85.9%) and $\mathbf{L_3}^{SS}$ (~100%). Therefore, the difference in the overall quantum yields (Q_{Ln}^{L}) is primarily ascribed to the disparate sensitization efficiencies exhibited by the ligands.

The enantiomeric nature of the assemblies was verified through the analysis of their circularly polarized luminescence

(CPL) spectra (Fig. 4D), suggesting the presence of a chiral environment surrounding the Eu^{III} center. Among these complexes, the largest luminescence dissymmetry factor (g_{lum}) for $Eu_4(\mathbf{L_2}^{SS})_6$ was calculated to be $+4.5 \times 10^{-2}$ (Fig. S78†), corresponding to the $^5D_0 \rightarrow {}^7F_1$ transition. This value is comparable to those

of previous mononuclear lanthanide complexes.[59,60] It can be inferred that the synergistic effect of ligands within the multinuclear rare earth cage contributes to an increase in the rigidity of the coordination environment of lanthanide ions, effectively increasing the magnitude of g_{lum}.[61]

Conclusions

In summary, subtle adjustments in the chelating arm not only enable the controllable synthesis of high-nuclear LOP edifices constructed by linear ligands but also lead to the efficient sensitization of lanthanide ion luminescence. The strategy of regulating the chelating angle and introducing auxiliary groups can effectively overcome the shortcoming of variable coordination orientations of lanthanide ions, providing a feasible pathway to construct multi-nuclear LOPs.

Experimental section

General

Unless otherwise stated, all chemicals and solvents were purchased from commercial companies and used as received. Deuterated solvents were obtained from Admas, J&K scientific, and Sigma-Aldrich. Triethylamine (TEA) was dried using CaH_2. The 1D and 2D-NMR spectra were measured on a Bruker Biospin Avance III (400 MHz) and JEOL ECZ600S (600 MHz) spectrometers. ^{1}H NMR chemical shifts were determined with respect to residual signals of the deuterated solvents used. ESI-TOF-MS spectra were recorded on an Impact II UHR-TOF mass spectrometer from Bruker, with tuning mix as the internal standard. Data analysis was conducted using the Bruker Data Analysis software (Version 4.3), and simulations were performed with the Bruker Isotope Pattern software. UV-Vis spectra were recorded on a UV-2700 UV-Visible spectrophotometer from SHIMADZU Corporation. Excitation and emission spectra were recorded on the FS5 spectrofluorometer from Edinburg Photonics. The microsecond emission lifetimes of solution samples were measured on an Edinburgh Instrument FLS980 spectrometer. Spectra were corrected for the experimental functions. Circular dichroism (CD) spectra were recorded on a MOS-450 circular dichroism spectrometer. Circularly polarized luminescence (CPL) measurements were performed with a JASCO CPL-200 spectrometer.

Synthesis of ligands $\mathbf{L}_n^{AC}$ (n = 1–3)

1,4-Diazidobenzene (108 mg, 1.0 mmol, 1.0 eq.), 6-ethynyl-*N*-isopropylpicolinamide (395 mg, 2.1 mmol, 2.1 eq.), sodium ascorbate (411 mg, 2.1 mmol, 2.1 eq.), and $CuSO_4{\cdot}5H_2O$ (225 mg, 0.9 mmol, 0.9 eq.) were added to a solution of DMF (60 mL). The reaction mixture was stirred at 60 °C for 48 h. After that, the reaction solution was cooled to room temperature, and the solvent was removed under reduced pressure. Then, 50 mL of EDTA-saturated aqueous solution was added and stirred for 1 h. The solution was extracted with an organic solvent mixture (50 mL × 3, DCM/MeOH, v/v 10/1), and the organic phase was washed with distilled water (30 mL × 2) and dried with anhydrous Na_2SO_4. The solvents were removed *in vacuo* to afford a crude product, which was further purified chromatographically (SiO_2, DCM/MeOH, v/v 100/1). The white powder $\mathbf{L_1}^{AC}$ was obtained after drying in vacuum (236 mg, 43.9%). ^{1}H NMR (400 MHz, $CDCl_3/CD_3OD$ v/v 5/1, 298 K) δ = 8.79 (s, 1H), 8.22 (d, J = 8.3 Hz, 1H), 8.19 (d, J = 8.8 Hz, 1H), 8.10 (d, J = 6.9 Hz, 1H), 8.07 (s, 2H), 7.94 (t, J = 7.8 Hz, 1H), 4.25 (m, J = 13.2, 6.6 Hz, 1H), 1.28 (d, J = 6.6 Hz, 6H). ^{13}C NMR (101 MHz, $CDCl_3/CD_3OD$ v/v 5/1, 298 K) δ = 163.60, 150.07, 148.40, 147.96, 138.68, 136.94, 123.09, 121.95, 120.53, 41.74, 22.54. ESI-TOF-MS for $C_{28}H_{28}N_{10}O_2$ $[M + Na]^+$: calcd, m/z = 559.2290; found, 559.2289.

$\mathbf{L_2}^{AC}$ was synthesized using a similar procedure, starting from 4,4′-diazidobiphenyl (80 mg, 0.34 mmol, 1.0 eq.). The white powder $\mathbf{L_2}^{AC}$ was obtained with a yield of 61.0% (127 mg). ^{1}H NMR (400 MHz, $CDCl_3/CD_3OD$ v/v 5/1, 298 K) δ = 8.68 (s, 2H), 8.27–8.14 (m, 4H), 8.11 (d, J = 7.5 Hz, 2H), 8.00–7.89 (m, 6H), 7.80 (d, J = 8.6 Hz, 4H), 4.25 (m, J = 13.2, 6.6 Hz, 2H), 1.28 (d, J = 6.6 Hz, 12H). ^{13}C NMR (101 MHz, $CDCl_3/CD_3OD$ v/v 5/1, 298 K) δ = 163.50, 149.97, 148.05, 140.42, 138.55, 136.40, 128.48, 123.00, 121.83, 121.16, 120.37, 41.55, 22.46. ESI-TOF-MS for $C_{34}H_{32}N_{10}O_2$ $[M + Na]^+$: calcd, m/z = 635.2605; found, 635.2602.

$\mathbf{L_3}^{AC}$ was synthesized with using a similar procedure, starting from 4,4′-diazidoterphenyl (235 mg, 1.25 mmol, 2.5 eq.). The white powder $\mathbf{L_3}^{AC}$ was obtained with a yield of 45.3% (156 mg). ^{1}H NMR (600 MHz, $CDCl_3/CD_3OD$ v/v 5/1, 298 K) δ = 8.67 (s, 1H), 8.16 (d, J = 7.8 Hz, 1H), 8.09 (d, J = 7.7 Hz, 1H), 7.93 (t, J = 6.5 Hz, 1H), 7.90 (d, J = 8.5 Hz, 2H), 7.80 (d, J = 10.9 Hz, 2H), 7.72 (s, 2H), 4.36–4.11 (m, 6.6 Hz, 1H), 1.27 (d, J = 6.6 Hz, 6H). ^{13}C NMR (151 MHz, $CDCl_3/CD_3OD$ v/v 5/1, 298 K) δ = 163.64, 149.97, 148.15, 147.97, 141.44, 139.19, 138.61, 136.04, 128.39, 127.71, 123.04, 121.82, 121.12, 120.55, 41.62, 22.44. ESI-TOF-MS for $C_{40}H_{36}N_{10}O_2$ $[M + Na]^+$: calcd, m/z = 711.2951; found, 711.2968.

Synthesis of ligands $\mathbf{L}_n^{SS/RR}$ (n = 1–3)

1,4-Diazidobenzene (160 mg, 1.0 mmol, 1.0 eq.) and $\mathbf{4}^{S}$ (901 mg, 3 mmol, 3.0 eq.) were added to a mixture of SA/sodium ascorbate (411 mg, 2.1 mmol, 2.1 equiv.) and $CuSO_4{\cdot}5H_2O$ (225 mg, 0.9 mmol, 0.9 eq.), and the mixture was stirred at 60 °C for 24 h. After filtration, the solvent was removed under vacuum distillation, and the crude product was purified chromatographically (SiO_2, DCM/MeOH 100/1) to afford $\mathbf{L_1}^{SS}$ as a pale yellow solid (456 mg, 59.9%). ^{1}H NMR (400 MHz, $CDCl_3/CD_3OD$ v/v 5/1, 298 K) δ = 8.59 (d, J = 8.5 Hz, 2H), 8.46 (s, 2H), 8.21 (d, J = 7.6 Hz, 4H), 8.11 (d, J = 8.4 Hz, 2H), 7.95 (t, J = 7.8 Hz, 2H), 7.80 (d, J = 7.9 Hz, 2H), 7.77 (s,

4H), 7.74 (d, J = 8.2 Hz, 2H), 7.59 (d, J = 7.1 Hz, 2H), 7.50–7.43 (m, 2H), 7.43–7.35 (m, 4H), 6.05 (p, J = 6.9 Hz, 2H), 1.77 (d, J = 6.8 Hz, 6H); ^{13}C NMR (101 MHz, $CDCl_3$/CD_3OD v/v 5/1, 298 K) δ = 163.24, 149.82, 148.14, 148.08, 138.53, 138.37, 136.58, 133.88, 131.15, 128.78, 128.33, 126.49, 125.82, 125.13, 123.38, 123.12, 122.84, 122.16, 121.54, 120.25, 45.21, 20.93; ESI-TOF-MS for $C_{57}H_{51}N_{15}O_3$ $[M + Na]^+$: calcd, m/z = 783.2915; found, 783.2910. $\mathbf{L_1}^{\mathbf{RR}}$ was synthesized in the same procedure as above, starting from $\mathbf{4}^{\mathbf{R}}$.

$\mathbf{L_2}^{\mathbf{SS}}$ was synthesized using a similar procedure, starting from 4,4′-diazidobiphenyl 4,4′-diazido-1,1′-biphenyl (236 mg, 1.0 mmol, 1.0 eq.). Pale yellow $\mathbf{L_2}^{\mathbf{SS}}$ was obtained with a yield of 75.1% (628 mg). ^{1}H NMR (400 MHz, $CDCl_3$, 298 K) δ = 8.41 (s, 2H), 8.37 (dd, J = 7.8, 0.8 Hz, 2H), 8.32 (d, J = 8.6 Hz, 2H), 8.27 (dd, J = 7.8, 0.8 Hz, 2H), 8.20 (d, J = 8.4 Hz, 2H), 8.00 (t, J = 7.8 Hz, 2H), 7.87 (d, J = 7.8 Hz, 2H), 7.82 (dd, J = 8.2, 6.3 Hz, 6H), 7.72 (d, J = 8.6 Hz, 4H), 7.64 (d, J = 7.1 Hz, 2H), 7.53 (t, J = 7.0 Hz, 2H), 7.47 (dd, J = 14.7, 7.2 Hz, 4H), 6.17–6.09 (m, 2H), 1.84 (d, J = 6.8 Hz, 6H); ^{13}C NMR (101 MHz, $CDCl_3$, 298 K) δ = 163.04, 149.76, 148.57, 148.11, 140.14, 138.44, 138.36, 136.40, 134.00, 131.27, 128.84, 128.45, 128.30, 126.60, 125.90, 125.20, 123.56, 123.18, 122.91, 122.04, 121.00, 119.99, 45.23, 21.11; ESI-TOF-MS for $C_{57}H_{51}N_{15}O_3$ $[M + Na]^+$: calcd, m/z = 859.3228; found, 859.3213. $\mathbf{L_2}^{\mathbf{RR}}$ was synthesized in the same procedure as above, starting from $\mathbf{4}^{\mathbf{R}}$.

$\mathbf{L_3}^{\mathbf{SS}}$ was synthesized using a similar procedure, starting from 4,4″-diazido-1,1′:4′,1″-terphenyl (312 mg, 1.0 mmol, 1.0 eq.). Pale yellow $\mathbf{L_3}^{\mathbf{SS}}$ was obtained with a yield of 55.0% (502 mg). ^{1}H NMR (400 MHz, $CDCl_3$, 298 K) δ = 8.40 (d, J = 8.6 Hz, 2H), 8.38 (s, 2H), 8.33 (d, J = 7.8 Hz, 2H), 8.24 (t, J = 8.1 Hz, 2H), 8.18 (d, J = 8.4 Hz, 2H), 7.95 (t, J = 7.8 Hz, 2H), 7.84 (d, J = 7.7 Hz, 2H), 7.78 (d, J = 8.2 Hz, 2H), 7.74 (d, J = 8.5 Hz, 4H), 7.70–7.59 (m, 10H), 7.50 (dd, J = 11.2, 4.1 Hz, 2H), 7.44 (dd, J = 16.3, 8.2 Hz, 4H), 6.16–6.06 (m, 2H), 1.83 (d, J = 6.8 Hz, 6H); ^{13}C NMR (101 MHz, $CDCl_3$, 298 K) δ = 163.11, 149.74, 148.61, 148.00, 140.89, 138.98, 138.41, 136.00, 133.97, 131.26, 128.83, 128.40, 128.09, 127.54, 126.57, 125.88, 125.19, 123.53, 123.12, 122.93, 121.98, 120.85, 120.05, 45.20, 29.72, 21.11. ESI-TOF-MS for $C_{57}H_{51}N_{15}O_3$ $[M + Na]^+$: calcd, m/z = 935.3541; found, 935.3531. $\mathbf{L_3}^{\mathbf{RR}}$ was synthesized in the same procedure as above, starting from $\mathbf{4}^{\mathbf{R}}$.

Synthesis of self-assembled complex of $\mathbf{L_1}^{\mathbf{AC}}$

To a white suspension of $\mathbf{L_1}^{\mathbf{AC}}$ (2.0 mg, 3.7 μmol, 1.0 eq.) in a solution of CD_3CN/CD_3OD (v/v 4/1, 500 μL), $Eu(OTf)_3$ (1.5 mg, 2.5 μmol, 0.67 eq.) was added and then stirred at 50 °C for 1 h. The light-yellow suspension gradually turned into a homogeneous yellow solution. This solution was characterized without further treatment. ^{1}H NMR (400 MHz, CD_3CN/CD_3OD v/v 4/1, 298 K) δ = 9.02 (s, 2H), 8.97 (s, 4H), 6.21 (t, J = 7.9 Hz, 2H), 5.97 (s, 2H), 5.28 (d, J = 7.5 Hz, 2H), 5.05 (d, J = 7.7 Hz, 2H), 3.97 (s, 1H), 3.06 (d, J = 4.6 Hz, 6H), 0.90 (d, J = 4.6 Hz, 6H). ^{13}C NMR (101 MHz, CD_3CN/CD_3OD v/v 4/1, 298 K) δ = 173.83, 152.37, 141.05, 136.20, 131.08, 122.91, 119.81, 95.58, 86.25, 44.84, 23.95, 22.19. ESI-TOF-MS for $Eu_4(\mathbf{L_1}^{\mathbf{AC}})_6(OTf)_{12}$: the following picked signals are those at the highest intensities. m/z calcd for $[Eu_4(\mathbf{L_1}^{\mathbf{AC}})_6(OTf)_4]^{8+}$ 552.8660, found 552.8663; calcd for $[Eu_4(\mathbf{L_1}^{\mathbf{AC}})_6(OTf)_5]^{7+}$ 653.1258, found 653.1260; calcd for $[Eu_4(\mathbf{L_1}^{\mathbf{AC}})_6(OTf)_6]^{6+}$ 787.8055, found 787.8057; calcd for $[Eu_4(\mathbf{L_1}^{\mathbf{AC}})_6(OTf)_7]^{5+}$ 974.1573, found 974.1572; calcd for $[Eu_4(\mathbf{L_1}^{\mathbf{AC}})_6(OTf)_8]^{4+}$ 1254.6845, found 1254.6846; $[Eu_4(\mathbf{L_1}^{\mathbf{AC}})_6(OTf)_9]^{3+}$ 1722.8971, found 1722.8948.

Synthesis of self-assembled complex of $\mathbf{L_2}^{\mathbf{AC}}$

To a white suspension of $\mathbf{L_2}^{\mathbf{AC}}$ (2.0 mg, 3.3 μmol, 1.0 eq.) in a solution of CD_3CN/CD_3OD (v/v 4/1, 500 μL), $Eu(OTf)_3$ (1.3 mg, 2.2 μmol, 0.67 eq.) was added and then stirred at 50 °C for 1 h. The light-yellow suspension gradually turned into a homogeneous yellow solution. This solution was characterized without further treatment. ^{1}H NMR (400 MHz, CD_3CN/CD_3OD v/v 4/1, 298 K) δ = 8.78 (s, 2H), 7.58 (d, J = 7.6 Hz, 4H), 7.53 (d, J = 7.6 Hz, 4H), 7.27 (t, J = 8.0 Hz, 2H), 6.32 (d, J = 7.2 Hz, 2H), 5.88 (d, J = 8.0 Hz, 2H), 4.23 (s, 2H), 1.55 (d, J = 4.4 Hz, 6H), 0.98 (d, J = 4.4 Hz, 6H). The ^{13}C NMR signals were too weak to be measured due to inhibition of structural transformation *via* low concentration of ligand. ESI-TOF-MS for $Eu_2(\mathbf{L_2}^{\mathbf{AC}})_3(OTf)_6$: the following picked signals are those at the highest intensities. m/z calcd for $[Eu_2(\mathbf{L_2}^{\mathbf{AC}})_3(OTf)_2]^{4+}$ 610.1398, found 610.1405; calcd for $[Eu_2(\mathbf{L_2}^{\mathbf{AC}})_3(OTf)_3]^{3+}$ 863.1706, found 863.1716; calcd for $[Eu_2(\mathbf{L_2}^{\mathbf{AC}})_3(OTf)_4]^{2+}$ 1369.2320, found 1369.2327. ESI-TOF-MS for $Eu_4(\mathbf{L_2}^{\mathbf{AC}})_6(OTf)_{12}$: m/z calcd for $[Eu_4(\mathbf{L_2}^{\mathbf{AC}})_6(OTf)_6]^{6+}$ 863.0038, found 863.0052; calcd for $[Eu_4(\mathbf{L_2}^{\mathbf{AC}})_6(OTf)_7]^{5+}$ 1065.3951, found 1065.3927; calcd for $[Eu_4(\mathbf{L_2}^{\mathbf{AC}})_6(OTf)_8]^{4+}$ 1368.9819, found 1368.9825.

Synthesis of self-assembled complex of $\mathbf{L_3}^{\mathbf{AC}}$

To a white suspension of $\mathbf{L_3}^{\mathbf{AC}}$ (4.0 mg, 5.8 μmol, 1.0 eq.) in a solution of CD_3CN/CD_3OD (v/v 4/1, 500 μL), $Eu(OTf)_3$ (2.3 mg, 3.9 μmol, 0.67 eq.) was added and then stirred at 50 °C for five minutes. The white suspension gradually turned into a homogeneous yellow solution. This solution was characterized without further treatment. ^{1}H NMR spectra showed the quantitative formation of $Eu_2(\mathbf{L_3}^{\mathbf{AC}})_3(OTf)_6$. ^{1}H NMR (600 MHz, CD_3CN/CD_3OD v/v 4/1, 298 K) δ = 8.76 (s, 1H), 7.58 (d, J = 10.8 Hz, 2H), 7.53 (d, J = 10.2 Hz, 2H), 7.33 (s, 3H), 6.38 (d, J = 6.0 Hz 1H), 5.96 (d, J = 9.6 Hz, 1H), 4.16 (s, 1H), 1.51 (s, 3H), 1.00 (s, 3H). ^{13}C NMR (151 MHz, CD_3CN/CD_3OD v/v 4/1, 298 K) δ = 174.51, 160.79, 153.88, 145.89, 142.57, 138.64, 134.03, 132.66, 128.10, 128.02, 120.85, 104.86, 96.88, 88.10, 44.12, 22.08, 21.90. ESI-TOF-MS for $Eu_2(\mathbf{L_3}^{\mathbf{AC}})_3(OTf)_6$: the following picked signals are those at the highest intensities. m/z calcd for $[Eu_2(\mathbf{L_3}^{\mathbf{AC}})_3(OTf)_1]^{5+}$ 503.7401, found 503.7407; calcd for $[Eu_2(\mathbf{L_3}^{\mathbf{AC}})_3(OTf)_2]^{4+}$ 666.9133, found 666.9136; calcd for $[Eu_2(\mathbf{L_3}^{\mathbf{AC}})_3(OTf)_3]^{3+}$ 939.2020, found 939.2018; calcd for $[Eu_2(\mathbf{L_3}^{\mathbf{AC}})_3(OTf)_4]^{2+}$ 1483.2793, found 1483.2794.

Synthesis of self-assembled complex of $\mathbf{L_1}^{\mathbf{SS}}$

To a white suspension of $\mathbf{L_1}^{\mathbf{SS}}$ (2.0 mg, 2.6 μmol, 1.0 eq.) in a solution of CD_3CN/CD_3OD (v/v 4/1, 500 μL), $Eu(OTf)_3$ (1.0 mg, 1.7 μmol, 0.67 eq.) was added and then stirred at 50 °C for 1 h. The white suspension turned into a homogeneous yellow solution. This solution was characterized without further treatment. ^{1}H NMR (400 MHz, CD_3CN/CD_3OD v/v 4/1, 298 K) δ = 9.57 (d, J = 8.1 Hz, 12H), 9.37 (s, 12H), 8.85 (s, 24H), 8.65 (s,

12H), 8.12 (t, J = 7.3 Hz, 12H), 7.57–7.41 (m, 24H), 6.94 (d, J = 8.3 Hz, 12H), 6.14 (t, J = 7.7 Hz, 12H), 5.53 (t, J = 7.9 Hz, 12H), 5.40 (d, J = 6.7 Hz, 12H), 4.34–4.16 (m, 24H), 2.36 (d, J = 5.5 Hz, 36H); ^{13}C NMR (101 MHz, CD_3CN/CD_3OD v/v 4/1, 298 K) δ = 171.02, 159.78, 150.93, 149.81, 140.40, 140.22, 135.96, 135.67, 133.57, 130.33, 129.98, 129.70, 127.68, 127.65, 126.78, 124.86, 123.36, 122.67, 122.54, 119.87, 119.36, 113.20, 103.93, 94.60, 91.46, 85.37, 82.09, 22.79. ESI-TOF-MS for $Eu_4(\mathbf{L_1}^{SS})_6(OTf)_{12}$: for $[Eu_4(\mathbf{L_1}^{SS})_6(OTf)_4]^{8+}$ calcd, m/z = 721.1636, found, 721.1652; for $[Eu_4(\mathbf{L_1}^{SS})_6(OTf)_5]^{7+}$ calcd, m/z = 845.4659, found, 845.4669; for $[Eu_4(\mathbf{L_1}^{SS})_6(OTf)_6]^{6+}$ calcd, m/z = 1011.2022, found, 1011.2031; for $[Eu_4(\mathbf{L_1}^{SS})_6(OTf)_7]^{5+}$ calcd, m/z = 1243.2332, found, 1243.2347; for $[Eu_4(\mathbf{L_1}^{SS})_6(OTf)_8]^{4+}$ calcd, m/z = 1591.2795, found, 1591.2808.

Complex of $\mathbf{L_1}^{RR}$ was prepared using the same procedure. Both ^{1}H NMR and ESI-TOF-MS demonstrated the formation of a pure-phase $Eu_4(\mathbf{L_1}^{RR})_6$ tetrahedron.

Synthesis of self-assembled complex of $\mathbf{L_2}^{SS}$

To a white suspension of $\mathbf{L_2}^{SS}$ (2.0 mg, 2.4 μmol, 1.0 eq.) in a solution of CD_3CN/CD_3OD (v/v 4/1, 500 μL), $Eu(OTf)_3$ (1.0 mg, 1.6 μmol, 0.67 equiv.) was added and then stirred at 50 °C for 1 h. The white suspension turned into a homogeneous yellow solution. This solution was characterized without further treatment. ^{1}H NMR (400 MHz, CD_3CN/CD_3OD v/v 4/1, 298 K) δ = 9.57 (d, J = 8.1 Hz, 12H), 9.37 (s, 12H), 8.85 (s, 24H), 8.65 (s, 12H), 8.12 (t, J = 7.3 Hz, 12H), 7.57–7.41 (m, 24H), 6.94 (d, J = 8.3 Hz, 12H), 6.14 (t, J = 7.7 Hz, 12H), 5.53 (t, J = 7.9 Hz, 12H), 5.40 (d, J = 6.7 Hz, 12H), 4.34–4.16 (m, 24H), 2.36 (d, J = 5.5 Hz, 36H); ^{13}C NMR (101 MHz, CD_3CN/CD_3OD v/v 4/1, 298 K) δ = 170.71, 150.74, 142.02, 140.41, 135.85, 134.18, 133.65, 130.01, 129.75, 129.11, 127.75, 127.60, 126.75, 124.94, 123.35, 122.47, 122.16, 119.90, 114.28, 103.42, 94.54, 85.13, 22.79. ESI-TOF-MS for $Eu_4(\mathbf{L_2}^{SS})_6(OTf)_{12}$ and $Eu_2(\mathbf{L_2}^{SS})_3(OTf)_{12}$: for $[Eu_4(\mathbf{L_2}^{SS})_6(OTf)_2]^{10+}$ calcd, m/z = 592.7593, found, 592.7594; for $[Eu_4(\mathbf{L_2}^{SS})_6(OTf)_3]^{9+}$ calcd, m/z = 675.1717, found, 675.1723; for $[Eu_4(\mathbf{L_2}^{SS})_6(OTf)_4]^{8+}$ calcd, m/z = 778.1872, found, 778.1869; for $[Eu_4(\mathbf{L_2}^{SS})_6(OTf)_5]^{7+}$ calcd, m/z = 910.6357, found, 910.6357; for $[Eu_4(\mathbf{L_2}^{SS})_6(OTf)_6]^{6+}$ calcd, m/z = 1087.2337, found, 1087.2337; for $[Eu_4(\mathbf{L_2}^{SS})_6(OTf)_7]^{5+}$ calcd, m/z = 1334.4709, found, 1334.4706; for $[Eu_2(\mathbf{L_2}^{SS})_3(OTf)_0]^{6+}$ calcd, m/z = 469.1406, found, 469.1415; for $[Eu_2(\mathbf{L_2}^{SS})_3(OTf)_1]^{5+}$ calcd, m/z = 592.7590, found, 592.7594; for $[Eu_2(\mathbf{L_2}^{SS})_3(OTf)_2]^{4+}$ calcd, m/z = 778.1871, found, 778.1869; for $[Eu_2(\mathbf{L_2}^{SS})_3(OTf)_3]^{3+}$ calcd, m/z = 1087.2336, found, 1087.2337; for $[Eu_2(\mathbf{L_2}^{SS})_3(OTf)_4]^{2+}$ calcd, m/z = 1705.3267, found, 1705.3273.

Complex of $\mathbf{L_2}^{RR}$ was prepared using the same procedure. Both ^{1}H NMR and ESI-TOF-MS demonstrated the formation of a mixture of $Eu_2(\mathbf{L_2}^{RR})_3$ and $Eu_4(\mathbf{L_2}^{RR})_6$, which coexisted in the solution. Increasing the concentration of $\mathbf{L_2}^{RR}$ led to a clearly identifiable pure-phase $Eu_4(\mathbf{L_2}^{RR})_6$ being observed in the ^{1}H NMR spectrum.

Synthesis of self-assembled complex of $\mathbf{L_3}^{SS}$

To a yellow suspension of $\mathbf{L_3}^{SS}$ (3.0 mg, 3.3 μmol, 1.0 eq.) in a solution of CD_3CN/CD_3OD (v/v 4/1, 500 μL), $Eu(OTf)_3$ (1.3 mg, 2.2 μmol, 0.67 eq.) was added and then stirred at 50 °C for 1 h. The yellow suspension turned into a homogeneous yellow solution. This solution was characterized without further treatment. ^{1}H NMR (400 MHz, CD_3CN/CD_3OD v/v 4/1, 298 K) δ = 8.48 (s, 6H), 8.09 (d, J = 8.2 Hz, 6H), 7.97 (d, J = 8.1 Hz, 6H), 7.75 (t, J = 7.3 Hz, 6H), 7.72–7.66 (m, 6H), 7.63 (d, J = 8.3 Hz, 6H), 7.42 (d, J = 8.2 Hz, 12H), 7.30 (d, J = 8.1 Hz, 12H), 7.20 (s, 12H), 7.05 (t, J = 7.7 Hz, 6H), 6.89 (d, J = 7.0 Hz, 6H), 6.63 (t, J = 8.0 Hz, 6H), 6.36 (s, 6H), 5.40 (d, J = 7.8 Hz, 6H), 5.26 (d, J = 7.8 Hz, 6H), 1.86 (d, J = 5.6 Hz, 18H); ^{13}C NMR (101 MHz, CD_3CN/CD_3OD v/v 4/1, 298 K) δ = 167.53, 160.20, 153.35, 142.78, 142.55, 140.18, 138.83, 134.67, 132.72, 130.58, 130.21, 128.58, 128.25, 128.13, 127.70, 127.10, 126.06, 123.01, 120.93, 32.50, 30.19, 22.26, 14.17. ESI-TOF-MS for $Eu_2(\mathbf{L_3}^{SS})_3(OTf)_6$: for $[Eu_2(\mathbf{L_3}^{SS})_3(OTf)_0]^{6+}$ calcd, m/z = 507.1563, found, 507.1578; for $[Eu_2(\mathbf{L_3}^{SS})_3(OTf)_1]^{5+}$ calcd m/z = 638.3781, found, 638.3789; for $[Eu_2(\mathbf{L_3}^{SS})_3(OTf)_2]^{4+}$ calcd m/z = 835.2107, found, 835.2121; for $[Eu_2(\mathbf{L_3}^{SS})_3(OTf)_3]^{3+}$ calcd m/z = 1163.2651, found, 1163.2667. Complex $\mathbf{L_3}^{RR}$ was prepared using the same procedure. Both ^{1}H NMR and ESI-TOF-MS demonstrated the formation of a pure-phase $Eu_2(\mathbf{L_3}^{RR})_3$ helicate.

Author contributions

Methodology: Xiao-Qing Guo and Qing-Fu Sun; investigation: Xiao-Qing Guo and Qing-Fu Sun; visualization: Xiao-Qing Guo; funding acquisition: Qing-Fu Sun; project administration: Qing-Fu Sun; supervision: Shao-Jun Hu and Li-Peng Zhou; writing – original draft: Xiao-Qing Guo and Qing-Fu Sun; writing – review and editing: Li-Peng Zhou, Shao-Jun Hu and Qing-Fu Sun.

Conflicts of interest

There are no conflicts to declare.

Acknowledgements

We thank the staff of the BL17B1 beamline at the National Centre for Protein Sciences Shanghai and Shanghai Synchrotron Radiation Facility (SSRF), Shanghai, People's Republic of China, for assistance during data collection. This work was supported by the National Key Research and Development Program of China (Grants 2021YFA1500400 and 2022YFA1503300), the National Natural Science Foundation of China (Grants 21825107, 22171264, and 22201285), the Science Foundation of Fujian Province (Grant 202lJ02016), and the Open Fund of Guangdong Provincial Key Laboratory of Functional Supramolecular Coordination Materials and Applications (2020B121201005).

References

1 J. M. Lehn, A. Rigault, J. Siegel, J. Harrowfield, B. Chevrier and D. Moras, *Proc. Natl. Acad. Sci. U. S. A.*, 1987, **84**, 2565.
2 M. Fujita, M. Tominaga, A. Hori and B. Therrien, *Acc. Chem. Res.*, 2005, **38**, 369.
3 P. Jin, S. J. Dalgarno and J. L. Atwood, *Coord. Chem. Rev.*, 2010, **254**, 1760.
4 T. R. Cook and P. J. Stang, *Chem. Rev.*, 2015, **115**, 7001.
5 D. A. Roberts, B. S. Pilgrim and J. R. Nitschke, *Chem. Soc. Rev.*, 2018, **47**, 626.
6 F.-F. Zhu, L.-J. Chen, S. Chen, G.-Y. Wu, W.-L. Jiang, J.-C. Shen, Y. Qin, L. Xu and H.-B. Yang, *Chem*, 2020, **6**, 2395.
7 S.-J. Bao, Z.-M. Xu, Y. Ju, Y.-L. Song, H. Wang, Z. Niu, X. Li, P. Braunstein and J.-P. Lang, *J. Am. Chem. Soc.*, 2020, **142**, 13356.
8 Y. Li, J. Dong, W. Gong, X. Tang, Y. Liu, Y. Cui and Y. Liu, *J. Am. Chem. Soc.*, 2021, **143**, 20939.
9 Y. Katagiri, Y. Tsuchida, Y. Matsuo and M. Yoshizawa, *J. Am. Chem. Soc.*, 2021, **143**, 21492.
10 K. Omoto, S. Tashiro and M. Shionoya, *J. Am. Chem. Soc.*, 2021, **143**, 5406.
11 L. J. Wang, S. Bai and Y.-F. Han, *J. Am. Chem. Soc.*, 2022, **144**, 16191.
12 S. M. Bierschenk, J. Y. Pan, N. S. Settineri, U. Warzok, R. G. Bergman, K. N. Raymond and F. D. Toste, *J. Am. Chem. Soc.*, 2022, **144**, 11425.
13 R. Banerjee, D. Chakraborty and P. S. Mukherjee, *J. Am. Chem. Soc.*, 2023, **145**, 7692.
14 A. C. Pearcy, L. S. Lisboa, D. Preston, N. B. Page, T. Lawrence, L. J. Wright, C. G. Hartinger and J. D. Crowley, *Chem. Sci.*, 2023, **14**, 8615.
15 H.-N. Zhang and G.-X. Jin, *Angew. Chem., Int. Ed.*, 2023, e202313605.
16 I. Regeni, R. Chowdhury, K. Terlinden, S. Horiuchi, J. J. J. Holstein, S. Feldmann and G. H. H. Clever, *Angew. Chem., Int. Ed.*, 2023, **62**, e202308288.
17 X. Z. Li, C. B. Tian and Q. F. Sun, *Chem. Rev.*, 2022, **122**, 6374.
18 Y. Zhou, H. Li, T. Zhu, T. Gao and P. Yan, *J. Am. Chem. Soc.*, 2019, **141**, 19634.
19 Y. B. Tan, Y. Okayasu, S. Katao, Y. Nishikawa, F. Asanoma, M. Yamada, J. Yuasa and T. Kawai, *J. Am. Chem. Soc.*, 2020, **142**, 17653.
20 H. L. Zhang, Y. Q. Zhai, H. Nojiri, C. Schroeder, H. K. Hsu, Y. T. Chan, Z. D. Fu and Y. Z. Zheng, *J. Am. Chem. Soc.*, 2022, **144**, 15193.
21 X.-F. Duan, L.-P. Zhou, H.-R. Li, S.-J. Hu, W. Zheng, X. Xu, R. Zhang, X. Chen, X.-Q. Guo and Q.-F. Sun, *J. Am. Chem. Soc.*, 2023, **145**, 23121.
22 B. Bocquet, G. Bernardinelli, N. Ouali, S. Floquet, F. Renaud, G. Hopfgartner and C. Piguet, *Chem. Commun.*, 2002, 930.
23 C. Piguet, *Chem. Commun.*, 2010, **46**, 6209.
24 J.-C. G. Bünzli, *Chem. Rev.*, 2010, **110**, 2729.
25 D. E. Barry, D. F. Caffrey and T. Gunnlaugsson, *Chem. Soc. Rev.*, 2016, **45**, 3244.
26 S. J. Butler and D. Parker, *Chem. Soc. Rev.*, 2013, **42**, 1652.
27 M. Bottrill, L. Kwok and N. J. Long, *Chem. Soc. Rev.*, 2006, **35**, 557.
28 T. K. Ronson, H. Adams, L. P. Harding, S. J. A. Pope, D. Sykes, S. Faulkner and M. D. Ward, *Dalton Trans.*, 2007, 1006.
29 B. E. Aroussi, S. Zebret, C. Besnard, P. Perrottet and J. Hamacek, *J. Am. Chem. Soc.*, 2011, **133**, 10764.
30 J. Wang, C. He, P. Wu, J. Wang and C. Duan, *J. Am. Chem. Soc.*, 2011, **133**, 12402.
31 G. Bozoklu, C. Gateau, D. Imbert, J. Pécaut, K. Robeyns, Y. Filinchuk, F. Memon, G. Muller and M. Mazzanti, *J. Am. Chem. Soc.*, 2012, **134**, 8372.
32 J. Hamacek, D. Poggiali, S. Zebret, B. El Aroussi, M. W. Schneider and M. Mastalerz, *Chem. Commun.*, 2012, **48**, 1281.
33 S. Han, H. Zhang, Y. J. Xie, L. L. Liu, C. F. Shan, X. K. Li, W. S. Liu and Y. Tang, *Appl. Surf. Sci.*, 2015, **328**, 368.
34 A. M. Johnson, C. A. Wiley, M. C. Young, X. Zhang, Y. Lyon, R. R. Julian and R. J. Hooley, *Angew. Chem., Int. Ed.*, 2015, **54**, 5641.
35 J. A. Kitchen, *Coord. Chem. Rev.*, 2017, **340**, 232.
36 T. Y. Bing, T. Kawai and J. Yuasa, *J. Am. Chem. Soc.*, 2018, **140**, 3683.
37 J. J. Lu, V. Montigaud, O. Cador, J. F. Wu, L. Zhao, X. L. Li, M. Guo, B. Le Guennic and J. K. Tang, *Inorg. Chem.*, 2019, **58**, 11903.
38 J. K. Zhong, L. Zhang, D. P. August, G. F. S. Whitehead and D. A. Leigh, *J. Am. Chem. Soc.*, 2019, **141**, 14249.
39 Z. W. Yao, Y. Y. Zhou, T. Gao, P. F. Yan and H. F. Li, *RSC Adv.*, 2021, **11**, 10524.
40 P. R. Su, T. Wang, P. P. Zhou, X. X. Yang, X. X. Feng, M. N. Zhang, L. J. Liang, Y. Tang and C. H. Yan, *Natl. Sci. Rev.*, 2022, **9**, nwab016.
41 X.-Q. Guo, L.-P. Zhou, S.-J. Hu, L.-X. Cai, P.-M. Cheng and Q.-F. Sun, *J. Am. Chem. Soc.*, 2021, **143**, 6202.
42 X. Yang, Z. Li, S. Wang, S. Huang, D. Schipper and R. A. Jones, *Chem. Commun.*, 2014, **50**, 15569.
43 S. Zebret, C. Besnard, G. Bernardinelli and J. Hamacek, *Eur. J. Inorg. Chem.*, 2012, **2012**, 2409.
44 Y. Y. Zhou, H. F. Li, T. Y. Zhu, T. Gao and P. F. Yan, *J. Am. Chem. Soc.*, 2019, **141**, 19634.
45 L.-L. Yan, C.-H. Tan, G.-L. Zhang, L.-P. Zhou, J.-C. Bunzli and Q.-F. Sun, *J. Am. Chem. Soc.*, 2015, **137**, 8550.
46 S.-J. Hu, X.-Q. Guo, L.-P. Zhou, L.-X. Cai and Q.-F. Sun, *Chin. J. Chem.*, 2019, **37**, 657.
47 D. L. Caulder and K. N. Raymond, *Acc. Chem. Res.*, 1999, **32**, 975.
48 X.-Z. Li, L.-P. Zhou, L.-L. Yan, D.-Q. Yuan, C.-S. Lin and Q.-F. Sun, *J. Am. Chem. Soc.*, 2017, **139**, 8237.
49 T. K. Ronson, H. Adams, L. P. Harding, S. J. A. Pope, D. Sykes, S. Faulkner and M. D. Ward, *Dalton Trans.*, 2007, 1006.

50 C.-T. Yeung, W. T. K. Chan, S.-C. Yan, K.-L. Yu, K.-H. Yim, W.-T. Wong and G.-L. Law, *Chem. Commun.*, 2015, **51**, 592.
51 C.-L. Liu, L.-P. Zhou, D. Tripathy and Q.-F. Sun, *Chem. Commun.*, 2017, **53**, 2459.
52 K.-H. Yim, C.-T. Yeung, M. R. Probert, W. T. K. Chan, L. E. Mackenzie, R. Pal, W.-T. Wong and G.-L. Law, *Commun. Chem.*, 2021, **4**, 116.
53 A. M. Castilla, M. A. Miller, J. R. Nitschke and M. M. J. Smulders, *Angew. Chem., Int. Ed.*, 2016, **55**, 10616.
54 J. Hamacek, S. Blanc, M. Elhabiri, E. Leize, A. Van Dorsselaer, C. Piguet and A.-M. Albrecht-Gary, *J. Am. Chem. Soc.*, 2003, **125**, 1541.
55 M. Elhabiri, J. Hamacek, J. Bünzli, G. Claude and A. M. Albrecht-Gary, *Eur. J. Inorg. Chem.*, 2004, **2004**, 51.
56 C. O. Kappe and E. Van der Eycken, *Chem. Soc. Rev.*, 2010, **39**, 1280.
57 J. A. Peters, J. Huskens and D. J. Raber, *Prog. Nucl. Magn. Reson. Spectrosc.*, 1996, **28**, 283.
58 P. W. Atkins and A. J. MacDermott, *J. Chem. Educ.*, 1982, **59**, 359.
59 J. P. Leonard, P. Jensen, T. McCabe, J. E. O'Brien, R. D. Peacock, P. E. Kruger and T. Gunnlaugsson, *J. Am. Chem. Soc.*, 2007, **129**, 10986.
60 K. T. Hua, J. Xu, E. E. Quiroz, S. Lopez, A. J. Ingram, V. A. Johnson, A. R. Tisch, A. de Bettencourt-Dias, D. A. Straus and G. Muller, *Inorg. Chem.*, 2012, **51**, 647.
61 J. I. Bruce, D. Parker, S. Lopinski and R. D. Peacock, *Chirality*, 2002, **14**, 562.